

Cite this: *J. Mater. Chem. C*, 2022,
10, 8719

The effects of the side-chain length of non-fullerene acceptors on their performance in all-small-molecule organic solar cells†

Fangfang Huang,^a Lingxian Meng,^a Changzun Jiang,^a Huazhe Liang,^a Yang Yang,^b Jian Wang,^b Xiangjian Wan,^b Chenxi Li,^a Zhaoyang Yao^a and Yongsheng Chen^{id}*^a

A series of acceptor–donor–acceptor type non-fullerene acceptors (NFAs), FC n -2Cl, with gradient substitution lengths of side chains (SCs) on molecular backbones, have been designed and synthesized for all-small-molecule organic solar cells (ASM-OSCs). The effects of SC length ranging from *n*-butyl to *n*-dodecyl on their optoelectronic properties, molecular packing, blend film morphology and overall photovoltaic performance have been systematically studied. Our results show that the BSFTR:FC10-2Cl-based ASM-OSC exhibited the best power conversion efficiency of over 12% due to its more efficient exciton dissociation, less charge recombination, balanced charge mobility and favorable morphology. Our work highlights the importance of fine-tuning the length of SCs of NFAs for further improving the performance of ASM-OSCs.

Received 20th March 2022,
Accepted 10th May 2022

DOI: 10.1039/d2tc01131j

rsc.li/materials-c

1. Introduction

In the past few decades, tremendous achievements have been made in power conversion efficiencies (PCEs) of solution-processed bulk-heterojunction organic solar cells (BHJ-OSCs) due to the merits such as light weight, low cost, flexibility, *etc.*^{1–5} Recently, the highest PCE has exceeded 19% for single-junction OSCs⁶ and 20% for tandem OSCs,⁷ both of which are based on polymer solar cells (PSCs). Nevertheless, polymers usually suffer from undefined molecular structures and batch-to-batch variation, which are detrimental to the industrialization of PSCs in the near future.^{8–12} All-small-molecule organic solar cells (ASM-OSCs) consisting of small-molecule donors (SMDs) and small-molecule acceptors (SMAs) have aroused increasing attention owing to their well-defined molecular structures, facile purification and outstanding batch-to-batch reproducibility, which renders ASM-OSCs more promising towards commercialization.^{13,14} Basically, ASM-OSCs are mainly divided into vapor-deposited^{15–20} and solution-processed

ASM-OSCs²¹ (the recent studies based on these two methods are roughly summarized in Tables S1 and S2 (ESI†), respectively). Among them, solution-processed ASM-OSCs have gained a lot of attention due to several prominent advantages, such as facile fabrication, large-area printing, roll-to-roll coating processes, *etc.*^{13,21,22} In recent years, solution-processed ASM-OSCs have brought remarkable achievements with the development of small-molecule materials and the optimization of device engineering.²³ For instance, Chen *et al.*²⁴ reported a series of oligothiophene-based SMDs, namely DCAE7T, DCAO7T and DCAEH7T. Among them, DCAO7T:PC₆₁BM-based ASM-OSCs yielded a PCE of 5.08%, which is the highest PCE for single-junction ASM-OSCs at that time. Subsequently, the benzo[1,2-*b*:4,5-*b'*] dithiophene (BDT) unit with a large and rigid planar conjugated structure was introduced in SMDs²⁵ and many high-performance SMDs were developed.¹⁴ Jones *et al.*²⁶ reported a BDT-based SMD, BTR, with nematic liquid crystalline behavior and the corresponding ASM-OSCs afforded a PCE of 9.3%. And then, Lu and co-workers developed a new liquid crystalline SMD by replacing the two bulky hexyl groups on the BDT unit of BTR with two chlorine (Cl) atoms, named BTR-Cl, which resulted in a remarkable PCE of 13.61% in ASM-OSCs with Y6 as the acceptor.²⁷ Hou *et al.*²⁸ developed another BDT-based SMD B1 by utilizing the phenyl unit as the side group of BDT, which led to an outstanding PCE of 15.3% in ASM-OSCs with BO-4Cl as the acceptor. Wei *et al.*²⁹ reported a new SMD ZR1 by extending the conjugated length of the BDT unit, achieving a decent PCE of 14.34% in ZR1:Y6-based ASM-OSCs. They also

^a State Key Laboratory and Institute of Elemento-Organic Chemistry, The Centre of Nanoscale Science and Technology and Key Laboratory of Functional Polymer Materials, Renewable Energy Conversion and Storage Center (RECAST), College of Chemistry, Nankai University, Tianjin, 300071, China. E-mail: yschen99@nankai.edu.cn

^b The Institute of Seawater Desalination and Multipurpose Utilization, Ministry of Natural Resources (Tianjin), Tianjin 300192, P. R. China

† Electronic supplementary information (ESI) available: Synthesis, TGA, UV spectroscopy, device fabrication and characterization, SCLC, AFM and TEM. See DOI: <https://doi.org/10.1039/d2tc01131j>

developed a novel SMD MPH-S based on the backbone of ZR1 and obtained an excellent PCE of 16.2% in MPH-S:BTP-eC9-based ASM-OSCs.³⁰ Moreover, the state-of-the-art single-junction ASM-OSCs have also exceeded 16% by using a ternary strategy.^{31,32} However, it is believed that the best PCE of ASM-OSCs is far from that achieved in view of the best PCE of over 19% already afforded by that of PSCs. Similar acceptor–donor–acceptor (A–D–A) structures and molecular sizes of active layer materials usually result in a very challenging control of bulk heterojunction morphologies in ASM-OSCs, which should be the most crucial issue needed to be addressed in future.^{30,33,34}

To conquer the great challenge mentioned above, most efforts have been focused on the molecular design of A–D–A type SMDs,^{27,35–40} specially, adjusting their alkyl chains. Wei and co-workers designed and synthesized three SMDs, namely, ZR2-C1-3, with different branching points of alkyl side chains on the dithieno[2,3-*d*:2',3'-*d'*]benzo[1,2-*b*:4,5-*b'*]dithiophene (DTBDT) unit.³³ The π - π stacking interactions of these three molecules were increased with the side-chain branching position moving away from core moiety. Finally, the ZR2-C3:Y6 based ASM-OSC afforded the highest PCE of 14.78% due to the matched crystallinities between D:A materials, which leads to an appropriate hierarchical morphology. Besides, Zhu *et al.* reported BDT3TR-SF⁴¹ and BSFTR³⁷ with different lengths and positions of alkyl chains on their π -bridges. A higher PCE of 13.69% was obtained by the ASM-OSC based on BSFTR:Y6 after optimizing through sequential solvent vapor (SVA) and thermal annealing (TA) treatment, which leads to the good crystallinity and favorable phase separation. In addition, in order to demonstrate that adjusting the length of alkyl chains on end groups

can effectively modify the molecular orientation, Hou *et al.*⁴² reported a series of SMDs, named DRTB-T-CX ($X = 2, 4, 6$ and 8). Among them, a top-performance of 11.24% was achieved by DRTB-T-C4:IT-4F-based ASM-OSCs.

In contrast to the modification of alkyl chains on SMDs, very less attention has been paid to fine-tuning the active layer morphology of ASM-OSCs by controlling the length of side chains on SMAs. But it is worth noting that the properties of SMAs also have a great influence on the performance of the corresponding ASM-OSCs. After all, the side engineering of NFAs is also an effective strategy for improving the PCEs of PSCs in many efficient systems,^{43–47} such as Y-series NFAs, IDT-series NFAs, *etc.* Herein, based on a non-fullerene acceptor (NFA) F-2Cl reported previously,⁴⁸ we designed and synthesized a series of NFAs, FC*n*-2Cl, with gradient substituent lengths of side chains ranging from *n*-butyl to *n*-dodecyl (Fig. 1(a)). A systematical study was carried out to discover the effects of side chain length on the molecular properties and the corresponding photovoltaic performance. The ASM-OSC performances based on the FC*n*-2Cl series NFAs are evaluated by blending with an SMD of BSFTR (Fig. 1(a)).⁴⁰ Among them, the highest PCE of 12.54% was achieved based on the *n*-decyl substituent FC10-2Cl acceptor, with an open-circuit voltage (V_{OC}) of 0.931 V, a short-circuit current density (J_{SC}) of 18.53 mA cm⁻², and a fill factor (FF) of 0.727. The outstanding performance of the BSFTR:FC10-2Cl system was mainly due to the more favorable morphology containing the mixed packing modes of both face-on and edge-on, which indicates the coexistence of vertical and parallel charge transportation channels in a BHJ device structure, thus rendering higher exciton

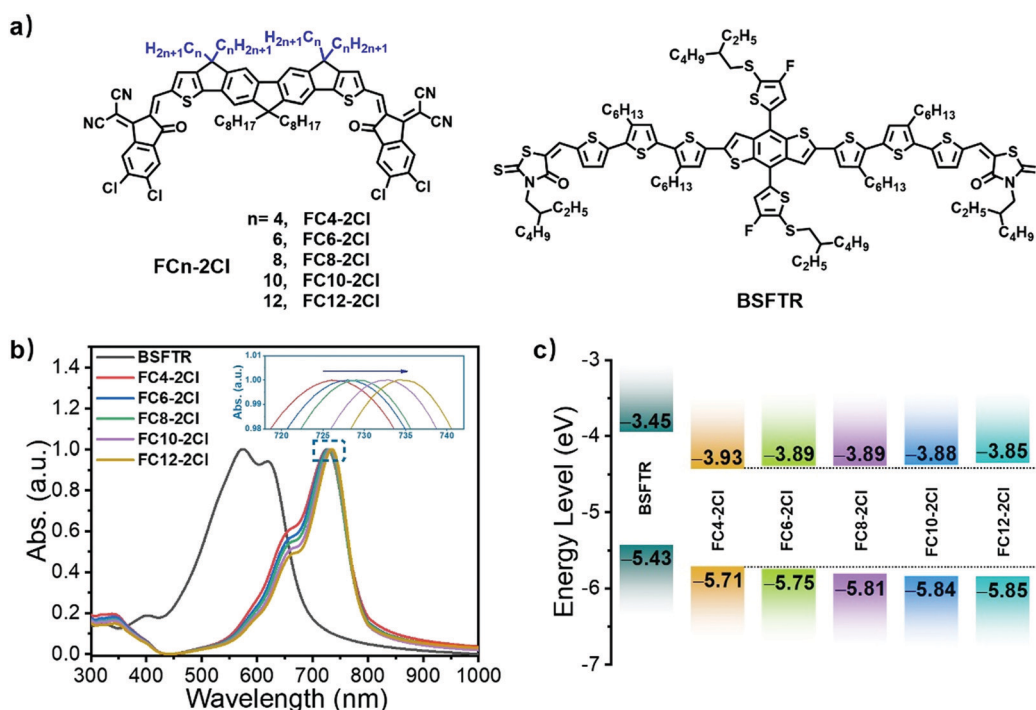


Fig. 1 (a) Chemical structures of FC*n*-2Cl and BSFTR; (b) normalized thin film optical absorption spectra of neat FC*n*-2Cl (the maximum absorption peaks are shown in the inset for clarity); (c) energy level diagrams for BSFTR and FC*n*-2Cl.

dissociation, more balanced hole/electron mobility ($\mu_{\text{h}}/\mu_{\text{e}}$) and less charge recombination. This result indicates that adjusting the side chain size of NFAs is also an effective strategy for further improving the performance of ASM-OSCs.

2. Results and discussion

2.1 Synthesis and characterization

The synthesis details of FC*n*-2Cl are provided in Scheme S1 (ESI†). We utilized a previous method to obtain the central core without side chains (compound 1).⁴⁹ And then, the nucleophilic substitution reactions of compound 1 with alkyl bromide chains of different lengths yielded compounds 2a–e. The intermediates 3a–e with two aldehyde groups were synthesized *via* the Vilsmeier–Haack reaction.⁵⁰ The subsequent Knoevenagel condensation reaction using bis(5,6-dichloro-3-oxo-2,3-dihydro-1*H*-indene-2,1-diylidene)*d*-imalononitrile (2ClIC) afforded the corresponding target compounds FC*n*-2Cl as dark-blue solids.⁵¹ The detailed synthesis procedures and full characterization using nuclear magnetic resonance (NMR) and high-resolution mass spectroscopy (HR-MS) of all compounds are shown in the ESI†, and FC*n*-2Cl shows good solubility in common solvents such as chlorobenzene (CB) and chloroform (CF).

The thermal behaviours of FC*n*-2Cl were measured by thermogravimetric analysis (TGA) and the thermal degradation temperature (T_{d} , 95% residue) of FC*n*-2Cl (~5 mg) was measured by TGA in the temperature range from 25 to 800 °C at a heating rate of 10 °C min⁻¹ under a N₂ atmosphere. As shown in Fig. S1 (ESI†), the TGA analysis shows that the onset points of the weight loss with 5% weight-loss temperature (T_{d}) of FC4-2Cl, FC6-2Cl, FC8-2Cl, FC10-2Cl and FC12-2Cl are 345, 333, 351, 334 and 335 °C, respectively. This indicates the high thermal stability of targeted NFAs under the N₂ atmosphere, which is an essential factor for the fabrication of ASM-OSCs.

2.2 Opto-electronic properties

The UV-vis absorption spectra of FC*n*-2Cl in dilute solution and on thin-films are provided in Fig. S2 (ESI†) and Fig. 1(b), and the detailed data are summarized in Table 1. In chloroform solution, all compounds show the same intense absorption from 500 to 800 nm, with a maximum peak located at 688 nm. However, in the solid film absorption, the longer the side chains on NFAs, the greater the red-shift of the maximum peak, which are further red-shifted after TA treatment. Besides, FC*n*-2Cl exhibits similar absorption edges, corresponding to the similar optical bandgaps of 1.52, 1.52, 1.53, 1.53 and 1.53 eV, respectively. Cyclic voltammetry (CV) measurements

were carried out to investigate the electrochemical properties of the five molecules (Fig. 1(c) and Table 1). The highest occupied molecular orbitals (HOMOs) shifted down from -5.71 to -5.85 eV and the lowest unoccupied molecular orbitals (LUMOs) shifted up from -3.93 to -3.85 eV as NFAs varied from FC4-2Cl to FC12-2Cl. The optical absorption and molecular orbital level results of the FC*n*-2Cl molecules indicate that the different lengths of the side chains on NFAs can influence the molecular solid packing behaviour and optoelectronic properties.

2.3 Molecular packing ability

To investigate the molecular packing ability for the FC*n*-2Cl, grazing-incidence wide angle X-ray scattering (GIWAXS) was performed and the 2D-GIWAXS patterns and line-cut profile information for neat films of FC*n*-2Cl are presented in Fig. 2 and Table S3 (ESI†). Owing to the similar chemical structures, all the molecules (annealed at 120 °C for 10 min) exhibited good molecular packing and preferential face-on packing mode because of the emergence of the (100) peak at $q_{xy} = 0.34\text{--}0.36 \text{ \AA}^{-1}$ in the in-plane (IP) direction and an obvious (010) peak at $q_z = 1.77\text{--}1.83 \text{ \AA}^{-1}$ in the out-of-plane (OOP) direction. The *d*-spacing values of the π - π stacking of FC4-2Cl, FC6-2Cl, FC8-2Cl, FC10-2Cl and FC12-2Cl can be calculated by $d = 2\pi/q$, which are 3.55, 3.49, 3.47, 3.45 and 3.43 Å, respectively. Remarkably, with an increase in the length of the side chains on NFAs, the *d*-spacing of the π - π stacking decreases gradually and the molecular stacking becomes tighter, which might be related to the interaction between side chains.⁵² However, no obvious influence on the (100) lamellar stacking distance was observed. As shown in Fig. 2(f), other obvious out-of-plane peaks at 0.95 \AA^{-1} (200, $d \sim 6.61 \text{ \AA}$) and 0.76 \AA^{-1} (300, $d \sim 8.27 \text{ \AA}$) appear in FC10-2Cl neat films, and 1.49 \AA^{-1} (200, $d \sim 4.22 \text{ \AA}$), 1.00 \AA^{-1} (300, $d \sim 6.28 \text{ \AA}$) and 0.93 \AA^{-1} (400, $d \sim 6.76 \text{ \AA}$) appear in FC12-2Cl neat films, suggesting the presence of longer-distance π - π stacking in their pristine films and more molecules stack regularly in the out-of-plane direction.^{53,54} Furthermore, estimated from the Scherrer equation,⁵⁵ crystal coherence length (CCL) values of (010) diffraction are 14.24, 24.59, 30.73, 30.90 and 35.34 Å for FC4-2Cl, FC6-2Cl, FC8-2Cl, FC10-2Cl and FC12-2Cl, respectively, indicating that these NFAs with longer side chains can form relatively larger (010) ordered stacking in their pristine films.⁵⁶ The discussion above is closely linked to the FF of the corresponding OSCs.

2.4 Photovoltaic device performance

Conventional devices with the structure of ITO/PEDOT:PSS/active layer/PDINO/Al (Fig. 3(a)) were fabricated and optimized

Table 1 The opto-electronic properties of FC*n*-2Cl

Acceptors	$\lambda_{\text{max}}^{\text{CF}}$ (nm)	$\lambda_{\text{max}}^{\text{film}}$ (nm)	$\lambda_{\text{max}}^{\text{film}}$ (TA) (nm)	$\lambda_{\text{edge}}^{\text{film}}$ (nm)	$E_{\text{g}}^{\text{opt}}$ (eV)	HOMO (eV)	LUMO (eV)	E_{g}^{CV} (eV)
FC4-2Cl	688	726	729	816	1.52	-5.71	-3.93	1.78
FC6-2Cl	688	728	735	815	1.52	-5.75	-3.89	1.86
FC8-2Cl	688	729	738	809	1.53	-5.81	-3.89	1.92
FC10-2Cl	688	733	745	810	1.53	-5.84	-3.88	1.96
FC12-2Cl	688	734	743	808	1.53	-5.85	-3.85	2.00

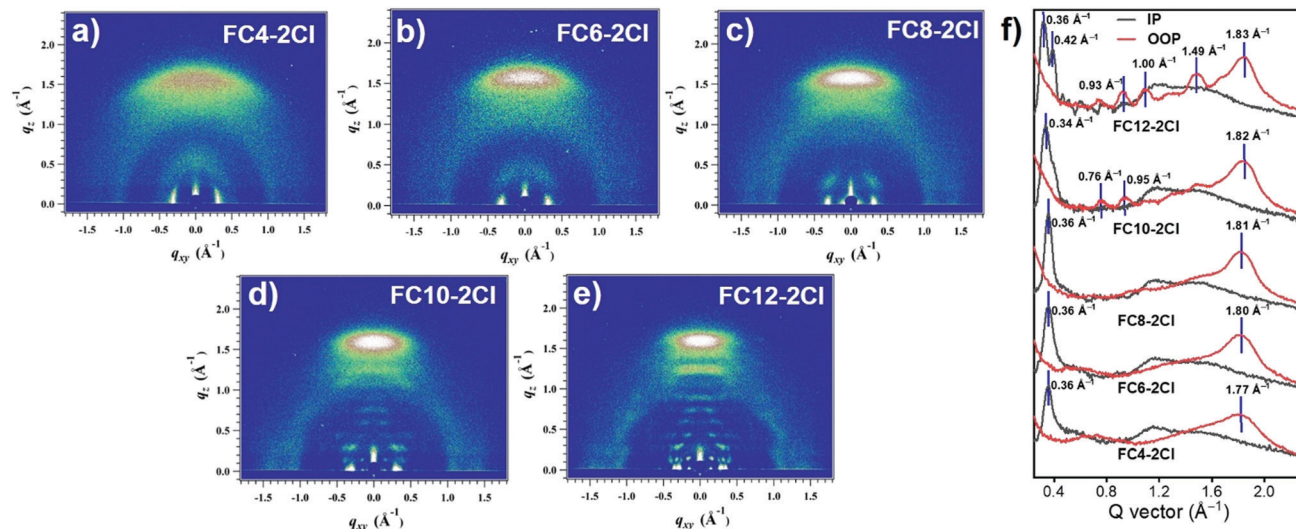


Fig. 2 (a)–(e) 2D-GIWAXS patterns and (f) in-plane and out-of-plane line-cut profiles of neat films for FC n -2Cl.

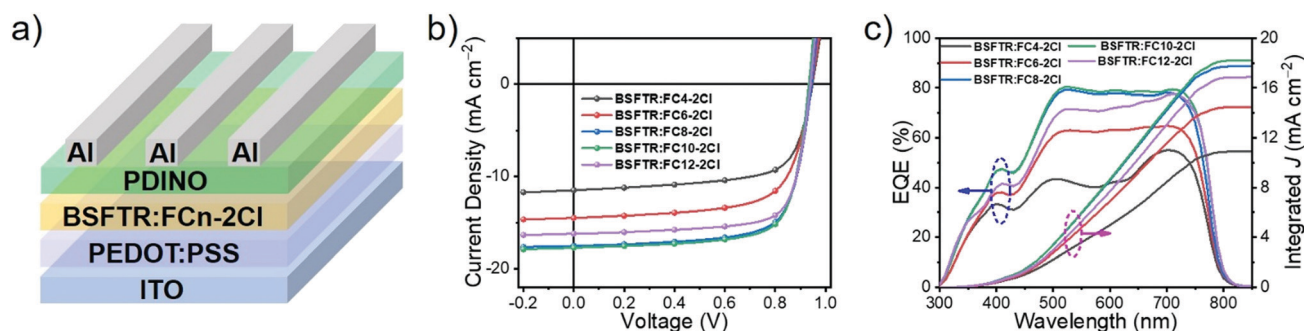


Fig. 3 (a) Device architecture of OSCs; (b) current-density–voltage (J – V) curves of OSCs based on BSFTR:FC n -2Cl under the illumination of AM 1.5G, 100 mW cm^{-2} ; (c) EQE curves of the corresponding OSCs.

Table 2 The optimized photovoltaic data of FC n -2Cl-based devices under the illumination of AM 1.5G (100 mW cm^{-2})

Devices	V_{OC}^a (V)	J_{SC}^a (mA cm^{-2})	Calc. J_{SC}^b (mA cm^{-2})	FF ^a	PCE ^a (%)
BSFTR:FC4-2Cl	0.944 ± 0.002 (0.948)	11.06 ± 0.36 (11.56)	10.91	0.691 ± 0.004 (0.696)	7.22 ± 0.15 (7.48)
BSFTR:FC6-2Cl	0.946 ± 0.002 (0.949)	14.36 ± 0.34 (14.77)	14.50	0.696 ± 0.008 (0.703)	9.53 ± 0.23 (9.85)
BSFTR:FC8-2Cl	0.938 ± 0.002 (0.942)	17.05 ± 0.37 (18.05)	17.76	0.722 ± 0.004 (0.729)	11.60 ± 0.17 (11.99)
BSFTR:FC10-2Cl	0.934 ± 0.003 (0.938)	17.74 ± 0.36 (18.53)	18.23	0.730 ± 0.005 (0.738)	12.12 ± 0.17 (12.54)
BSFTR:FC12-2Cl	0.939 ± 0.004 (0.944)	16.30 ± 0.26 (16.83)	16.87	0.739 ± 0.006 (0.750)	11.11 ± 0.23 (11.47)

^a The PCE values were calculated from 15 devices; the values in parentheses are the parameters of the best FC n -2Cl-based devices. ^b The J_{SC} values integrated from the EQE spectra.

to evaluate the photovoltaic properties using FC n -2Cl as acceptors. The wide-bandgap SMD BSFTR⁴⁰ was employed as the donor blending with FC n -2Cl. The photovoltaic parameters and J – V curves of the optimized devices are collected in Table 2 and Fig. 3(b), respectively. OSCs based on BSFTR:FC n -2Cl blend films afford comparable V_{OC} values around 0.940 V. The J_{SC} values are continuously increased from 11.06 ± 0.36 to $17.74 \pm 0.36 \text{ mA cm}^{-2}$ by increasing the lengths of side chains from 4 to 10, but decreased with n -dodecyl. And FFs continue to increase as the side chains of NFAs lengthens. After optimization (Tables S4–S18 (ESI[†])), a champion device based on

BSFTR:FC10-2Cl delivers the highest PCE of 12.54%. Besides, despite the similar absorption range, the FC n -2Cl-based OSCs exhibited different J_{SC} s, which can be observed from their EQE results shown in Fig. 3(c). Such a difference might be caused by their different exciton separation, charge extraction, transport, recombination and collection, which will be discussed below.

2.5 Device characterization

In order to obtain more information and further demonstrate the reasons for the best performance of the BSFTR:FC10-2Cl-based device, we systematically carried out a series of physical

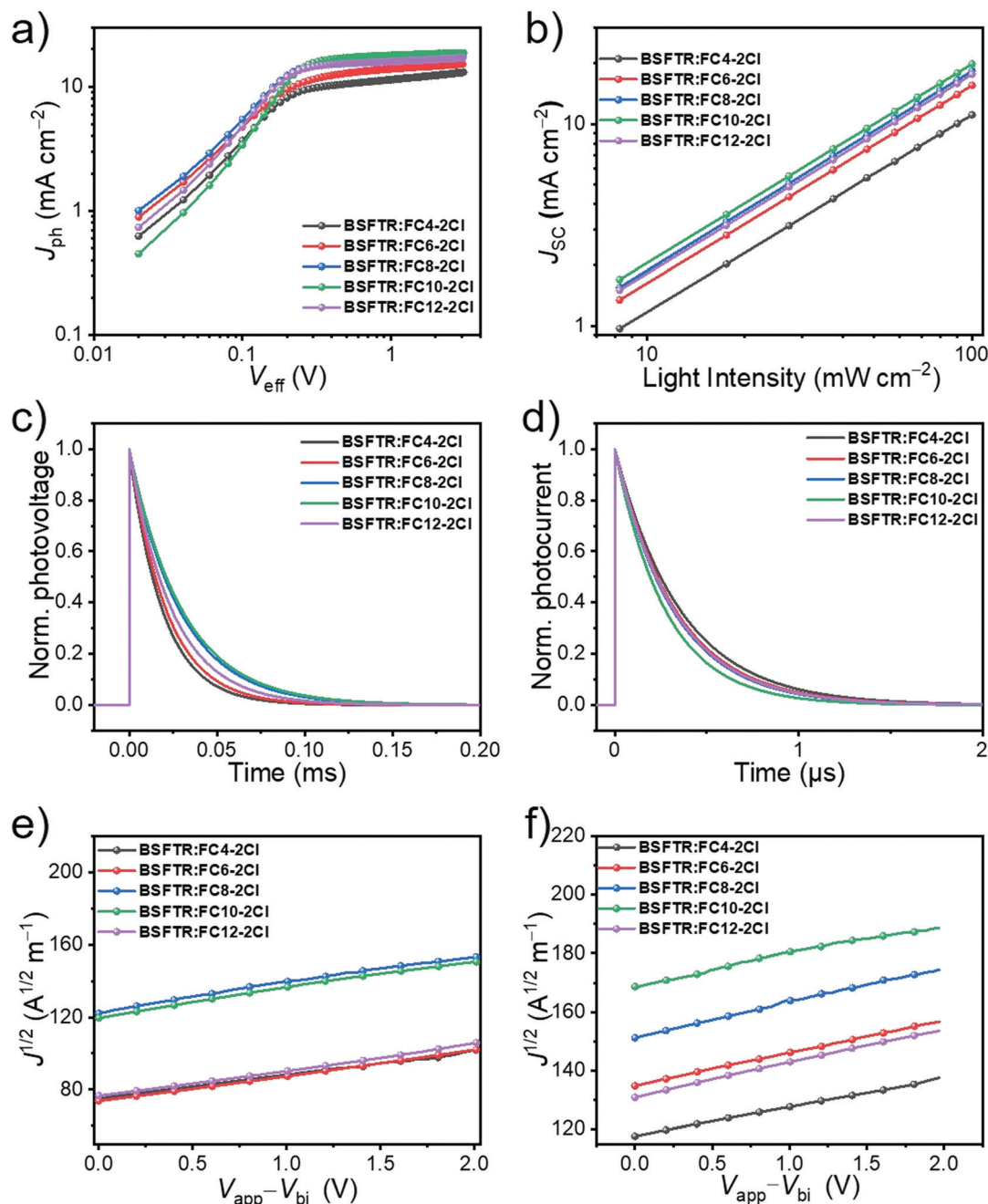


Fig. 4 (a) Plots of J_{ph} vs. V_{eff} ; (b) light intensity (P) dependence of J_{sc} ; (c) normalized transient photovoltage and (d) normalized transient photocurrent measurements; the $J^{1/2}$ - V plots for the (e) hole-only and (f) electron-only devices; all the measurements above were based on OSCs of BSFTR:FCn-2Cl.

dynamics characterization. First, to study the exciton dissociation and charge collection properties, the plots of the photocurrent density (J_{ph}) versus effective voltage (V_{eff}) were recorded. Herein, $J_{ph} = J_L - J_D$, where J_L and J_D are the current density under illumination and in the dark, respectively. The $V_{eff} = V_0 - V_a$, where V_a is the applied voltage and V_0 is the voltage at $J_{ph} = 0$. As displayed in Fig. 4(a) and Table S19 (ESI[†]), all the devices achieved saturated current densities (J_{sat}) when V_{eff} reaches ~ 2.0 V, indicating the minimized charge recombination at higher voltages.^{43,57} The value of P_{diss} , which is the ratio

of J_{ph} to the saturation photocurrent density (J_{sat}) of the device under the short-circuit conditions, represents charge dissociation probability.⁵⁸ The P_{diss} values for FC4-2Cl, FC6-2Cl, FC8-2Cl and FC10-2Cl are continuously increased from 88% to 92%, 96% and 96%, but P_{diss} for FC12-2Cl is decreased to 94%. The charge collection probability (P_{coll}) calculated using the ratio of J_{ph} to J_{sat} under the maximum power output conditions⁵⁸ showed the same trend as P_{diss} . The values of P_{coll} for FC4-2Cl, FC6-2Cl, FC8-2Cl and FC10-2Cl are continuously increased from 71% to 74%, 83% and 84%, but P_{coll} for FC12-2Cl is

a BHJ device structure, which facilitates intermolecular charge transfer and eventually results in the excellent J_{SC} in the ASM-OSCs.^{62,63}

Moreover, the translation of packing mode may be caused by the miscibility between SMDs and NFAs. To investigate their miscibility, we measured the contact angle and calculated their surface tension for neat films of all materials and the interfacial tensions for the corresponding blend films (Fig. 5(g)–(p), Fig. S5 (ESI[†]) and Table S20 (ESI[†])) based on the literature method.⁶⁴ According to the contact angle, the pure film of FC4-2Cl with the shortest side chains exhibits the highest surface tension while the pure film of FC12-2Cl with the longest side chains exhibits the lowest surface tension. And then, the equation $\chi \propto (\sqrt{\gamma_{donor}} - \sqrt{\gamma_{acceptor}})^2$ was used to further compare the miscibility of the blend films, which was suggested by Moons and co-workers in which χ is the Flory–Huggins parameter.⁶⁵ The χ values of BSFTR:FC n -2Cl (from $n = 4$ to 6, 8, 10 and 12) blend films are 2.63, 1.12, 0.99, 0.59 and 0.52, respectively, indicating that the blend of BSFTR:FC12-2Cl exhibits the best miscibility, the most orderly and closely packed.³⁰ Highly ordered packing makes the BSFTR:FC12-2Cl-based ASM-OSCs exhibit high FF. However, overly good miscibility may cause reduced domain purity,^{59,66,67} which have a strong impact on exciton separation, charge extraction, transport, recombination and collection, thus decreasing its J_{SC} .

The results mentioned above can be further confirmed by transmission electron microscopy (TEM) and atomic force microscopy (AFM). In TEM images, for the BSFTR:FC n -2Cl ($n = 4$ and 6) blend films (Fig. S6a and b, ESI[†]), the light domains were apparently considerably larger and looser, which results from their low miscibility. As shown in Fig. S6c–e (ESI[†]), the better miscibility and more orderly packing lead to the alternately smaller light and dark regions for the blend films of BSFTR:FC n -2Cl ($n = 8, 10, \text{ and } 12$). For the BSFTR:FC10-2Cl blend film, more favourable phase separation and more appropriate morphology were observed. And in the AFM images, the values of root-mean-square (RMS) are 4.94, 1.78, 1.19, and 1.00 nm, as NFAs varied from FC4-2Cl to FC6-2Cl, FC8-2Cl and FC10-2Cl, respectively. Compared with the RMS of the BSFTR:FC10-2Cl blend film, the BSFTR:FC12-2Cl blend film exhibited a coarser surface (RMS = 1.63 nm), further corroborating its better packing ability,³⁰ which is consistent with the discussion of GIWAXS and miscibility.

3. Conclusion

In summary, a series of NFAs, FC n -2Cl ($n = 4, 6, 8, 10$ and 12), with gradient substituent lengths of side chains, have been synthesized to shed light on the possible significant effects of side chain lengths on the performance of ASM-OSCs. The blend film of FC10-2Cl with n -decyl side chains affords more favourable morphology due to the mixed packing modes containing face-on and edge-on, which indicates the coexistence of vertical and parallel charge transportation channels in a BHJ device structure, thus rendering the higher exciton dissociation, more

balanced hole/electron mobility (μ_h/μ_e) and less charge recombination. Finally, the ASM-OSC utilizing BSFTR:FC10-2Cl as the active layer exhibited the champion PCE of 12.54%. Our work unveils that the side chain lengths of NFAs in ASM-OSCs could have a great influence on the light absorption and energy levels of thin films, molecular packing modes and charge dynamics, thus resulting in much different photovoltaic performance. Therefore, it has been proved that the side chain modulation of NFAs should be also an effective strategy for improving the PCE of ASM-OSCs.

Author contributions

Y. C. developed the concept and designed the experiments. Y. C., C. L., Z. Y. and X. W. supervised and directed the project. F. H. performed the chemical synthesis and property characterization of NFAs, carried out the device fabrication and measurements, analysed the experimental data and prepared the manuscript. L. M. helped in designing the project. C. J. measured the ¹³C NMR of target compounds. H. L. calculated the Flory-Huggins parameters. Y. Y. and J. W. performed the GIWAXS measurements.

Conflicts of interest

The authors declare no conflicts of interest.

Acknowledgements

The authors gratefully acknowledge the financial support from NSFC (21935007, 52025033, 51873089, 52103218), MoST (2019YFA0705900) of China, and Tianjin city (20JCZDJC00740) and the 111 Project (B12015).

References

- 1 J. K. Ho, S. K. So, S.-W. Liu and K.-T. Wong, *Mater. Sci. Eng., R*, 2018, **124**, 1–57.
- 2 S. B. Darling and F. You, *RSC Adv.*, 2013, **3**, 17633.
- 3 J. Hou, O. Inganäs, R. H. Friend and F. Gao, *Nat. Mater.*, 2018, **17**, 119–128.
- 4 C. Jiao, Z. Guo, B. Sun, Y.-q-q Yi, L. Meng, X. Wan, M. Zhang, H. Zhang, C. Li and Y. Chen, *J. Mater. Chem. C*, 2020, **8**, 6293–6298.
- 5 Y. Sun, M. Chang, L. Meng, X. Wan, H. Gao, Y. Zhang, K. Zhao, Z. Sun, C. Li, S. Liu, H. Wang, J. Liang and Y. Chen, *Nat. Electron.*, 2019, **2**, 513–520.
- 6 Y. Cui, Y. Xu, H. F. Yao, P. Q. Bi, L. Hong, J. Q. Zhang, Y. F. Zu, T. Zhang, J. Z. Qin, J. Z. Ren, Z. H. Chen, C. He, X. T. Hao, Z. X. Wei and J. H. Hou, *Adv. Mater.*, 2021, **33**, e2102420.
- 7 Z. Zheng, J. Wang, P. Bi, J. Ren, Y. Wang, Y. Yang, X. Liu, S. Zhang and J. Hou, *Joule*, 2022, **6**, 171–184.
- 8 R. Z. Liang, Y. Zhang, V. Savikhin, M. Babics, Z. Kan, M. Wohlfahrt, N. Wehbe, S. Liu, T. Duan, M. F. Toney,

- F. Laquai and P. M. Beaujuge, *Adv. Energy Mater.*, 2018, **9**, 1802836.
- 9 H. Tang, H. Chen, C. Yan, J. Huang, P. W.-K. Fong, J. Lv, D. Hu, R. Singh, M. Kumar, Z. Xiao, Z. Kan, S. Lu and G. Li, *Adv. Energy Mater.*, 2020, **10**, 2001076.
- 10 B. Kan, M. Li, Q. Zhang, F. Liu, X. Wan, Y. Wang, W. Ni, G. Long, X. Yang, H. Feng, Y. Zuo, M. Zhang, F. Huang, Y. Cao, T. P. Russell and Y. Chen, *J. Am. Chem. Soc.*, 2015, **137**, 3886–3893.
- 11 J. Zhou, Y. Zuo, X. Wan, G. Long, Q. Zhang, W. Ni, Y. Liu, Z. Li, G. He, C. Li, B. Kan, M. Li and Y. Chen, *J. Am. Chem. Soc.*, 2013, **135**, 8484–8487.
- 12 Q. Zhang, B. Kan, F. Liu, G. Long, X. Wan, X. Chen, Y. Zuo, W. Ni, H. Zhang, M. Li, Z. Hu, F. Huang, Y. Cao, Z. Liang, M. Zhang, T. P. Russell and Y. Chen, *Nat. Photonics*, 2014, **9**, 35–41.
- 13 Y. Huo, H.-L. Zhang and X. Zhan, *ACS Energy Lett.*, 2019, **4**, 1241–1250.
- 14 H. Tang, C. Yan, J. Huang, Z. Kan, Z. Xiao, K. Sun, G. Li and S. Lu, *Matter*, 2020, **3**, 1403–1432.
- 15 P. Sullivan, A. Duraud, I. Hancox, N. Beaumont, G. Mirri, J. H.-R. Tucker, R. A. Hatton, M. Shipman and T. S. Jones, *Adv. Energy Mater.*, 2011, **1**, 352–355.
- 16 B. Verreet, B. P. Rand, D. Cheyens, A. Hadipour, T. Aernouts, P. Heremans, A. Medina, C. G. Claessens and T. Torres, *Adv. Energy Mater.*, 2011, **1**, 565–568.
- 17 H. Gommans, T. Aernouts, B. Verreet, P. Heremans, A. Medina, C. G. Claessens and T. Torres, *Adv. Funct. Mater.*, 2009, **19**, 3435–3439.
- 18 C. W. Tang, *Appl. Phys. Lett.*, 1986, **48**, 183–185.
- 19 D. Park, I. H. Jung, S.-Y. Jang and S. Yim, *Macromol. Res.*, 2019, **27**, 444–447.
- 20 J. Lee, D. Park, I. Heo and S. Yim, *Mater. Res. Bull.*, 2014, **58**, 132–135.
- 21 C. He and J. Hou, *Acta Phys.-Chim. Sin.*, 2018, **34**, 1202–1210.
- 22 S. Park, T. Kim, S. Yoon, C. W. Koh, H. Y. Woo and H. J. Son, *Adv. Mater.*, 2020, **32**, 2002217.
- 23 C. Xu, Z. Zhao, K. Yang, L. Niu, X. Ma, Z. Zhou, X. Zhang and F. Zhang, *J. Mater. Chem. A*, 2022, **10**, 6291–6329.
- 24 Y. Liu, X. Wan, F. Wang, J. Zhou, G. Long, J. Tian, J. You, Y. Yang and Y. Chen, *Adv. Energy Mater.*, 2011, **1**, 771–775.
- 25 Y. Liu, X. Wan, F. Wang, J. Zhou, G. Long, J. Tian and Y. Chen, *Adv. Mater.*, 2011, **23**, 5387–5391.
- 26 K. Sun, Z. Xiao, S. Lu, W. Zajaczkowski, W. Pisula, E. Hanssen, J. M. White, R. M. Williamson, J. Subbiah, J. Ouyang, A. B. Holmes, W. W.-H. Wong and D. J. Jones, *Nat. Commun.*, 2015, **6**.
- 27 H. Chen, D. Hu, Q. Yang, J. Gao, J. Fu, K. Yang, H. He, S. Chen, Z. Kan, T. Duan, C. Yang, J. Ouyang, Z. Xiao, K. Sun and S. Lu, *Joule*, 2019, **3**, 3034–3047.
- 28 J. Qin, C. An, J. Zhang, K. Ma, Y. Yang, T. Zhang, S. Li, K. Xian, Y. Cui, Y. Tang, W. Ma, H. Yao, S. Zhang, B. Xu, C. He and J. Hou, *Sci. China: Chem.*, 2020, **63**, 1142–1150.
- 29 R. Zhou, Z. Jiang, C. Yang, J. Yu, J. Feng, M. A. Adil, D. Deng, W. Zou, J. Zhang, K. Lu, W. Ma, F. Gao and Z. Wei, *Nat. Commun.*, 2019, **10**.
- 30 L. Zhang, X. Zhu, D. Deng, Z. Wang, Z. Zhang, Y. Li, J. Zhang, K. Lv, L. Liu, X. Zhang, H. Zhou, H. Ade and Z. Wei, *Adv. Mater.*, 2022, **34**, e2106316.
- 31 J. Qin, Z. Chen, P. Bi, Y. Yang, J. Zhang, Z. Huang, Z. Wei, C. An, H. Yao, X. Hao, T. Zhang, Y. Cui, L. Hong, C. Liu, Y. Zu, C. He and J. Hou, *Energy Environ. Sci.*, 2021, **14**, 5903–5910.
- 32 M. Jiang, H. Bai, H. Zhi, L. Yan, H. Y. Woo, L. Tong, J. Wang, F. Zhang and Q. An, *Energy Environ. Sci.*, 2021, **14**, 3945–3953.
- 33 R. Zhou, Z. Jiang, Y. Shi, Q. Wu, C. Yang, J. Zhang, K. Lu and Z. Wei, *Adv. Funct. Mater.*, 2020, **30**, 2005426.
- 34 J. Ge, L. Hong, W. Song, L. Xie, J. Zhang, Z. Chen, K. Yu, R. Peng, X. Zhang and Z. Ge, *Adv. Energy Mater.*, 2021, **11**, 2100800.
- 35 J. Subbiah, C. J. Lee, V. D. Mitchell and D. J. Jones, *ACS Appl. Mater. Interfaces*, 2021, **13**, 1086–1093.
- 36 H. Bin, J. Yao, Y. Yang, I. Angunawela, C. Sun, L. Gao, L. Ye, B. Qiu, L. Xue, C. Zhu, C. Yang, Z. G. Zhang, H. Ade and Y. Li, *Adv. Mater.*, 2018, **30**, e1706361.
- 37 Q. Yue, H. Wu, Z. Zhou, M. Zhang, F. Liu and X. Zhu, *Adv. Mater.*, 2019, **31**, e1904283.
- 38 H. Tang, T. Xu, C. Yan, J. Gao, H. Yin, J. Lv, R. Singh, M. Kumar, T. Duan, Z. Kan, S. Lu and G. Li, *Adv. Sci.*, 2019, **6**, 1901613.
- 39 H. Li, Y. Zhao, J. Fang, X. Zhu, B. Xia, K. Lu, Z. Wang, J. Zhang, X. Guo and Z. Wei, *Adv. Energy Mater.*, 2018, **8**, 1702377.
- 40 H. Wu, Q. Yue, Z. Zhou, S. Chen, D. Zhang, S. Xu, H. Zhou, C. Yang, H. Fan and X. Zhu, *J. Mater. Chem. A*, 2019, **7**, 15944–15950.
- 41 H. Wu, H. Fan, S. Xu, L. Ye, Y. Guo, Y. Yi, H. Ade and X. Zhu, *Small*, 2019, **15**, e1804271.
- 42 L. Yang, S. Zhang, C. He, J. Zhang, Y. Yang, J. Zhu, Y. Cui, W. Zhao, H. Zhang, Y. Zhang, Z. Wei and J. Hou, *Chem. Mater.*, 2018, **30**, 2129–2134.
- 43 X. Zhang, Y. Q. Ding, H. R. Feng, H. H. Gao, X. Ke, H. T. Zhang, C. X. Li, X. J. Wan and Y. S. Chen, *Sci. China: Chem.*, 2020, **63**, 1799–1806.
- 44 S. Chen, L. Feng, T. Jia, J. Jing, Z. Hu, K. Zhang and F. Huang, *Sci. China: Chem.*, 2021, **64**, 1192–1199.
- 45 C. Kim, S. Chen, J. S. Park, G.-U. Kim, H. Kang, S. Lee, T. N.-L. Phan, S.-K. Kwon, Y.-H. Kim and B. J. Kim, *J. Mater. Chem. A*, 2021, **9**, 24622–24630.
- 46 Y. Chen, T. Liu, L.-K. Ma, W. Xue, R. Ma, J. Zhang, C. Ma, H. K. Kim, H. Yu, F. Bai, K. S. Wong, W. Ma, H. Yan and Y. Zou, *J. Mater. Chem. A*, 2021, **9**, 7481–7490.
- 47 T. Liu, Y. Zhang, Y. Shao, R. Ma, Z. Luo, Y. Xiao, T. Yang, X. Lu, Z. Yuan, H. Yan, Y. Chen and Y. Li, *Adv. Funct. Mater.*, 2020, **30**, 2000456.
- 48 Y. Zhang, H. Feng, L. Meng, Y. Wang, M. Chang, S. Li, Z. Guo, C. Li, N. Zheng, Z. Xie, X. Wan and Y. Chen, *Adv. Energy Mater.*, 2019, **9**, 1902688.
- 49 C.-Y. Chang, Y.-J. Cheng, S.-H. Hung, J.-S. Wu, W.-S. Kao, C.-H. Lee and C.-S. Hsu, *Adv. Mater.*, 2012, **24**, 549–553.
- 50 N. L. Qiu, H. J. Zhang, X. J. Wan, C. X. Li, X. Ke, H. R. Feng, B. Kan, H. T. Zhang, Q. Zhang, Y. Lu and Y. S. Chen, *Adv. Mater.*, 2017, **29**, 1604964.

- 51 Y. Wang, Y. Wang, B. Kan, X. Ke, X. Wan, C. Li and Y. Chen, *Adv. Energy Mater.*, 2018, **8**, 1802021.
- 52 H. Chen, X. Xia, J. Yuan, Q. Wei, W. Liu, Z. Li, C. Zhu, X. Wang, H. Guan, X. Lu, Y. Li and Y. Zou, *ACS Appl. Mater. Interfaces*, 2021, **13**, 36053–36061.
- 53 X. Li, H. Huang, I. Angunawela, J. Zhou, J. Du, A. Liebman-Pelaez, C. Zhu, Z. Zhang, L. Meng, Z. Xie, H. Ade and Y. Li, *Adv. Funct. Mater.*, 2019, **30**, 1906855.
- 54 G. Zhang, X. K. Chen, J. Xiao, P. C.-Y. Chow, M. Ren, G. Kupgan, X. Jiao, C. C.-S. Chan, X. Du, R. Xia, Z. Chen, J. Yuan, Y. Zhang, S. Zhang, Y. Liu, Y. Zou, H. Yan, K. S. Wong, V. Coropceanu, N. Li, C. J. Brabec, J. L. Bredas, H. L. Yip and Y. Cao, *Nat. Commun.*, 2020, **11**, 3943.
- 55 T. Miyazaki and T. Sasaki, *Nucl. Technol.*, 2017, **194**, 111–116.
- 56 Q. Ma, Z. Jia, L. Meng, J. Zhang, H. Zhang, W. Huang, J. Yuan, F. Gao, Y. Wan, Z. Zhang and Y. Li, *Nano Energy*, 2020, **78**, 105272.
- 57 S. Li, Y. Sun, B. Zhou, Q. Fu, L. Meng, Y. Yang, J. Wang, Z. Yao, X. Wan and Y. Chen, *ACS Appl. Mater. Interfaces*, 2021, **13**, 40766–40777.
- 58 P. W.-M. Blom, V. D. Mihailetschi, L. J.-A. Koster and D. E. Markov, *Adv. Mater.*, 2007, **19**, 1551–1566.
- 59 Z. Zhang, H. Wang, J. Yu, R. Sun, J. Xu, L. Yang, R. Geng, J. Cao, F. Du, J. Min, F. Liu and W. Tang, *Chem. Mater.*, 2020, **32**, 1297–1307.
- 60 A. Baumann, J. Lorrman, D. Rauh, C. Deibel and V. Dyakonov, *Adv. Mater.*, 2012, **24**, 4381–4386.
- 61 A. Maurano, R. Hamilton, C. G. Shuttle, A. M. Ballantyne, J. Nelson, B. O'Regan, W. Zhang, I. McCulloch, H. Azimi, M. Morana, C. J. Brabec and J. R. Durrant, *Adv. Mater.*, 2010, **22**, 4987–4992.
- 62 T. Kumari, S. M. Lee, S.-H. Kang, S. Chen and C. Yang, *Energy Environ. Sci.*, 2017, **10**, 258–265.
- 63 H. Bin, Y. Yang, Z. G. Zhang, L. Ye, M. Ghasemi, S. Chen, Y. Zhang, C. Zhang, C. Sun, L. Xue, C. Yang, H. Ade and Y. Li, *J. Am. Chem. Soc.*, 2017, **139**, 5085–5094.
- 64 K.-H. Kim, H. Kang, H. J. Kim, P. S. Kim, S. C. Yoon and B. J. Kim, *Chem. Mater.*, 2012, **24**, 2373–2381.
- 65 S. Nilsson, A. Bernasik, A. Budkowski and E. Moons, *Macromolecules*, 2007, **40**, 8291–8301.
- 66 L. Ye, H. Hu, M. Ghasemi, T. Wang, B. A. Collins, J.-H. Kim, K. Jiang, J. H. Carpenter, H. Li, Z. Li, T. McAfee, J. Zhao, X. Chen, J. L.-Y. Lai, T. Ma, J.-L. Bredas, H. Yan and H. Ade, *Nat. Mater.*, 2018, **17**, 253–260.
- 67 L. Ye, B. A. Collins, X. Jiao, J. Zhao, H. Yan and H. Ade, *Adv. Energy Mater.*, 2018, **8**, 1703058.